PERGAMON

Solid-State Electronics 43 (1999) 1429–1436

SOLID-STATE ELECTRONICS

Comparison of conventional and thermally-stable cascode (TSC) AlGaAs/GaAs HBTs for microwave power applications

Shawn S.H. Hsu[a,*], Burhan Bayraktaroglu[b], Dimitris Pavlidis[a]

[a]*Department of Electrical Engineering and Computer Science, The University of Michigan, Ann Arbor, MI 48109-2122, USA*
[b]*Northrop Grumman Corporation, Baltimore, MD 21203, USA*

Abstract

Conventional and thermally-stable cascode HBT (TSC-HBT) were fabricated using a self-aligned emitter-base process on MOCVD-grown wafers. The pronounced self-heating effect of conventional AlGaAs/GaAs HBT was reduced dramatically by the cascode design approach. The DC, small and large-signal characteristics of conventional common–emitter (CE) and TSC-HBTs were compared and a direct assessment of the new HBT design is provided.

1. Introduction

AlGaAs/GaAs heterojunction bipolar transistors (HBTs) have been implemented for a wide range of power applications such as power amplifiers and mixers. However, the low thermal conductivity of the material causes pronounced thermal effects, which are an important issue for power applications. To control these effects, various approaches have been used in the past including ballast resistors and thermal-shunt structures [1–3]. More recently, a new Thermally-Stable Cascode HBT (TSC-HBT) design was developed, which not only provides an effective solution to the thermal runaway issue, but also can improve the robustness of high power HBTs under overstressed DC or RF bias conditions [4]. The TSC-HBT employs the cascode configuration to regulate the current in each emitter finger independently. In other words, the cascode HBTs reduce the undesired thermal effects by locating the current and power generation regions into separate temperature zones.

In this paper, the performance of conventional and cascode HBTs are compared under dc, small-signal and large-signal conditions. In addition, a Gummel–Poon based model including thermal sub-circuit and behavior sources is used to simulate the junction temperature increase and to provide a clearer picture of device characteristic [5,6]. Conventional HBTs with identical characteristics to the common–emitter (CE) stage of the cascode configuration are used for comparison. The large-signal model of the cascode configuration also used two single HBT stages with identical characteristics to those of conventional HBTs. We found that TSC-HBT, in addition to being more robust, can provide higher power gain and efficiency than the conventional HBTs at microwave frequencies.

2. Device design and fabrication

A TSC-HBT is made up of a CE and a CB stage connected as shown in Fig. 1. In such a device, the CB

* Corresponding author.
E-mail address: shuohung@engin.umich.edu (S.S.H. Hsu)

0038-1101/99/$ - see front matter
PII: S0038-1101(99)00085-4

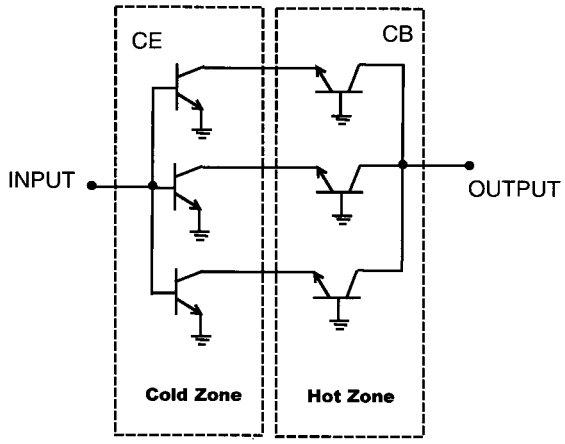

Fig. 1. Schematic drawing of a TSC-HBT cell showing individual connection between CE and CB stages.

stage that provides the output power (and therefore becomes hot) is physically separated from the part that regulates the current (CE-stage). Because the electro-thermal feedback is effectively eliminated in this configuration, the collector current remains uniformly distributed across all parts of the CB stage. The net result is that a uniform temperature distribution is achieved at all DC and RF drive levels without thermal instability. As shown by the results of this paper, this increased thermal stability is possible without compromising the microwave performance of power HBT cells.

All devices studied here were fabricated on MOCVD-grown 100-mm diameter wafers with a self-aligned emitter-base process. A constant emitter geometry $2.5 \times 20\ \mu m^2$ was used in all designs. The conventional CE HBT had four emitter fingers separated by 30 μm. A similar layout configuration was used for the CE and the CB stages of the cascode cell with 100 μm separation between the stages. This separation distance was found from computer simulations to be sufficient to provide thermal isolation between the stages. To increase the thermal stability, thermal shunt structures were used for both the conventional HBT and the CE stage of the TSC-HBT. The thermal shunt structure provides stronger thermal coupling between adjacent emitter fingers and therefore can minimize the variation in the current value of each emitter finger of the cell. In the case of the conventional HBT, the thermal shunt approach alleviates the thermal runaway conditions and allows higher power operation. For a TSC-HBT, the thermal shunt serves to minimize the temperature difference between the emitter fingers of the CE stage to ensure a uniform collector current supply to the CB stage. No separate thermal-shunt structure was used for the CB stage. The final substrate thickness was 100 μm for all devices.

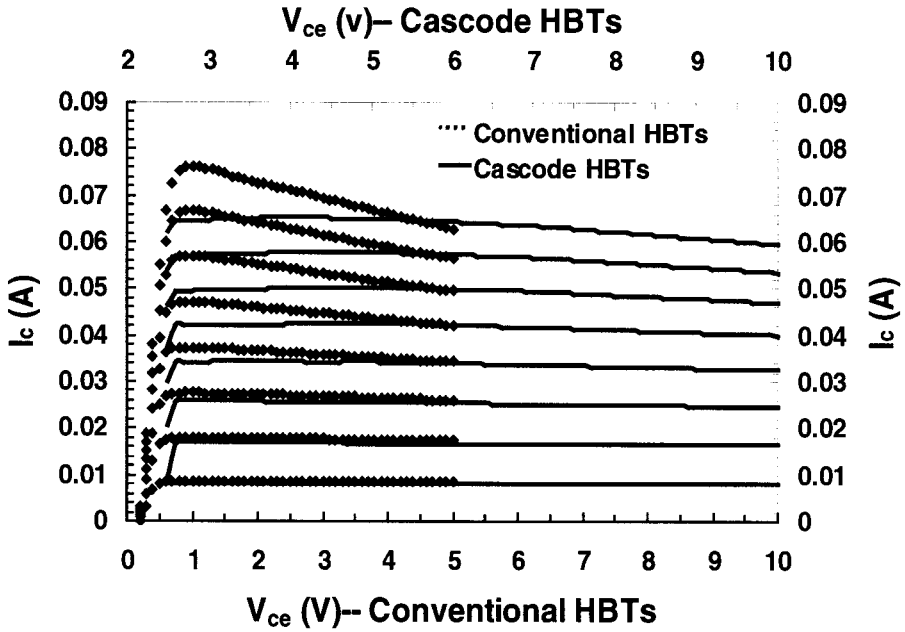

Fig. 2. Forward I_c– V_{ce} characteristics for conventional and cascode HBTs. $I_b = 0.3, 0.6, \ldots, 2.4$ mA, $V_{ce} = 0$–5 V for conventional HBT and 2.5–10 V for cascode HBTs.

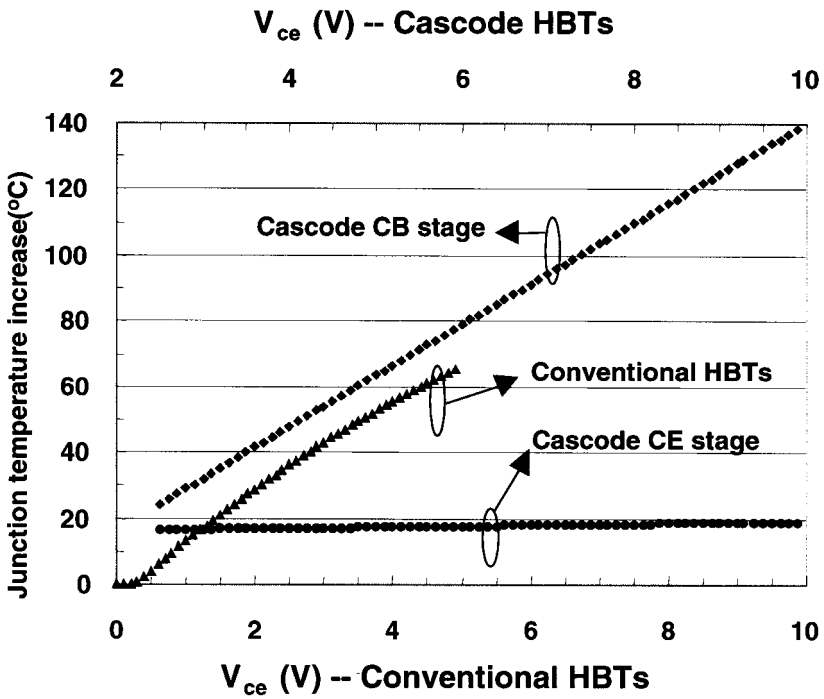

Fig. 3. Simulated junction temperature increase for conventional, cascode CE stage and CB stage HBTs. $I_b = 2.4$ mA, $V_{ce} = 0$–5 V for conventional HBTs and 2.5–10 V for cascode HBTs.

An identical cell layout approach was used in TSC-HBTs for both CE and CB stages. Virtually complete thermal isolation was provided between CE and CB stages by separating these cells by at least 100 μm. Thermal shunt structures were used for the CE stage to minimize the temperature variation between emitter fingers and therefore maintain a uniform collector current generation. The collector of each CE subcell was directly connected to the corresponding emitter of the CB subcell. No thermal shunt structures were used for the CB stage cell.

We compared the performance of 4-finger cells (4-finger subcells for the CE and CB stages for TSC-HBT) throughout this paper. Additional information was provided for larger devices to confirm that the superior microwave performance of TSC-HBT can be extended to higher power levels.

3. Experimental results and discussion

3.1. DC characteristics

The room temperature I_c– V_{ce} characteristic of conventional and cascode HBTs under constant I_b bias condition are shown in Fig. 2. A negative slope of the collector current in the forward I_c– V_{ce} characteristics of conventional devices indicates the strong influence of junction temperature on current gain. The reverse hole-current injection increase with the junction temperature is the main reason causing a reduced gain under constant I_b bias [5]. A similar effect was not observed in TSC-HBTs because the rise in temperature is confined mostly to the CB cell, whose current is controlled by the CE cell located at a cooler temperature zone. As can be seen, the collector current of the conventional HBT dropped by about 15 mA at $I_b = 2.4$ mA, $V_{ce} = 5$ V due to the thermal effect. On the other hand, the TSC-HBT suffered considerably less from the thermal effects; I_c dropped by about 6 mA at $I_b = 2.4$ mA, even when the collector voltage was increased to 10 V.

A large-signal microwave device model including self-heating effects was employed to investigate the thermal characteristics of both devices. A temperature controlled current source was employed to model the increase in the reverse hole injection from the base to emitter, while a temperature controlled voltage source was used to describe the decrease in the emitter junction built-in potential. In addition, a thermal subcircuit including a current source and a thermal resistance were used to obtain a self-consistent thermal HBT model. In the sub-circuit, the current source describes the device power consumption and the voltage drop in

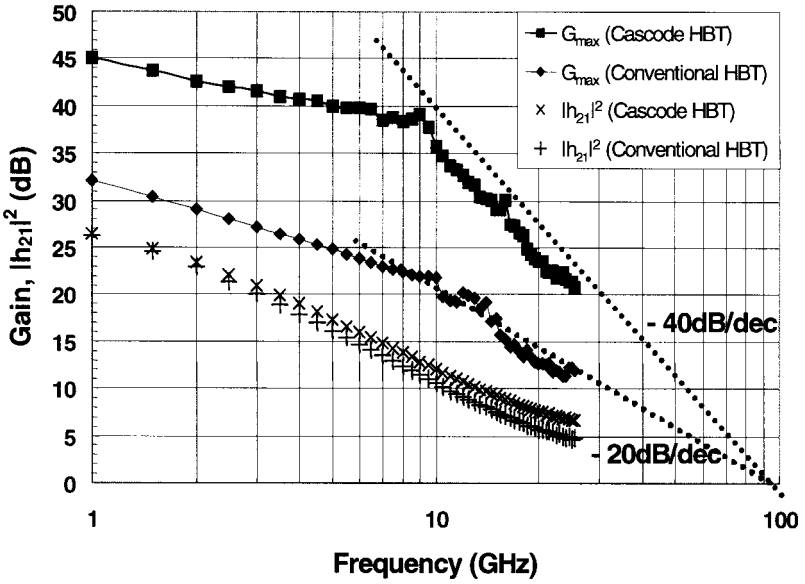

Fig. 4. G_{max} and $|h_{21}|^2$ for conventional and cascode HBTs. $I_b = 2.4$ mA, $I_c = 65.06$ mA, $V_{ce} = 4$ V for conventional HBTs; $I_b = 2.1$ mA, $V_{b2} = 2.5$ V, $I_c = 57.44$ mA, $V_{ce} = 7$ V for cascode HBTs.

the thermal resistance presents the junction temperature increase. The parameters for this physical-based model were extracted from the Gummel-plot, I_c– V_{ce} characteristics under both constant I_b and V_{be} conditions and from the small-signal S-parameters [7]. A large-signal model was developed first for conventional devices and then applied to the cascode configuration. Good agreement was obtained between measured and simulated results.

Based on the developed large-signal models, the base–emitter junction temperature increase of conventional HBTs and cascode CE, CB stages were extracted from the output of the thermal sub-circuit and the results are shown in Fig. 3. The TSC-HBT CE stage junction temperature was found to increase by ~20°C at $V_{ce} = 10$ V, while the temperature increase was ~60°C for the conventional HBT at $V_{ce} = 5$ V. As can be seen, the junction temperature of the cascode CB-stage was somewhat higher than that of the CE-stage at all power dissipation levels. This is due to the fact that the main voltage drop occurs across the CB stage, which therefore, consumes the largest amount of power.

Since most of the collector voltage dropped on the CB stage and the CE and CB stages were thermally isolated, the current control stage could be kept at lower temperature in the cascode HBTs even under high power consumption conditions. These results highlight the advantages of the TSC-HBT design to suppress electrothermal effects by maintaining a lower junction temperature increase at the CE stage.

3.2. Microwave small-signal characteristics

The small-signal S-parameters of the conventional and TSC-HBT devices were measured using an automated network analyzer (HP8510C) in the frequency range of 0.5–25.5 GHz. The MSG (maximum stable gain), MAG (maximum available gain) and $|h_{21}|^2$ versus frequency characteristics are shown in Fig. 4 for both the conventional and the TSC-HBT. The bias conditions corresponding to the highest f_{max} were $I_b = 2.4$ mA, $I_c = 65.06$ mA, $V_{ce} = 4$ V for conventional HBTs and $I_b = 2.1$ mA, $V_{b2} = 2.5$ V (base voltage for CB-stage), $I_c = 57.44$ mA, $V_{ce} = 7$ V for cascode device. The maximum stable gain for TSC-HBT devices is ~13 dB higher than for conventional HBTs at lower frequencies. Above 10 GHz, G_{max} dropped at different slopes (−20 dB/dec and −40 dB/dec for CE and TSC-HBT, respectively). Obviously, the common–base stage provided extra gain to the cascode configuration, but caused a sharper decrease in gain–frequency characteristics. The extrapolated results suggest a similar f_{max} value of ~92 GHz for both devices. On the other hand, $|h_{21}|^2$ is higher for TSC-HBTs in the measured frequency range (0.5–25.5 GHz) leading to higher f_t. The higher value of f_t for cascode devices is due to lower bias voltage applied to the CE stage compared to the bias applied to the conventional HBT.

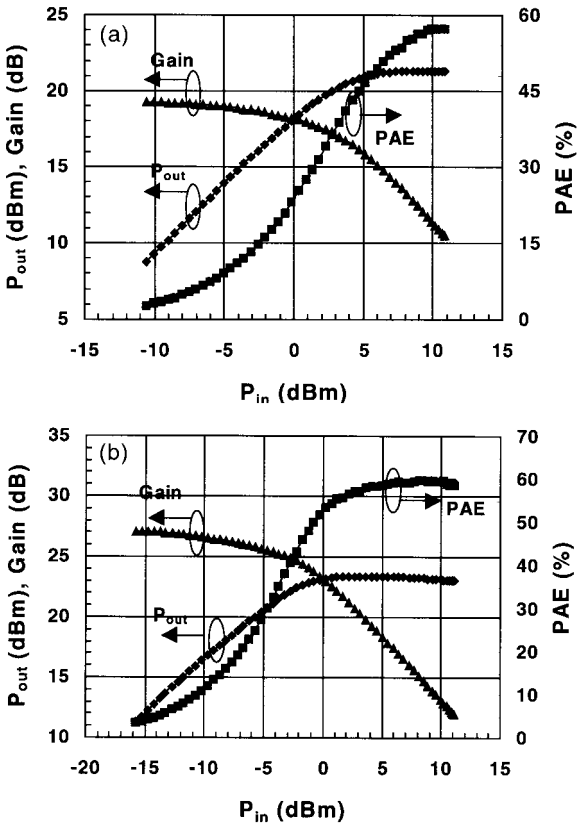

Fig. 5. Load-pull measurement of conventional and cascode HBTs (a) Gain, P_{out} and PAE for conventional HBTs (b) Gain, P_{out} and PAE for cascode HBTs.

3.3. Large-signal power performance

On-wafer power characterization was performed at 8 GHz using a load-pull measurement system with electromechanical tuners, which provide the ability to control the input and output impedances. The power performance such as gain, power-added efficiency and output power were evaluated. In addition, load-pull contour measurements were performed to provide a clearer picture of the device power characteristics. The devices were biased under the same conditions as above. The input and output impedances were optimized for maximum gain at $P_{in}=0$ dBm. The corresponding source (Γ_s) and load (Γ_L) reflection coefficients were $\Gamma_s=0.793\angle-173.3^\circ$ and $\Gamma_L=0.254\angle105.6^\circ$ for the conventional HBTs; $\Gamma_s=0.793\angle-173.3^\circ$ and $\Gamma_L=0.539\angle77.7^\circ$ for the cascode HBTs. Fig. 5 shows the measured gain, PAE and P_{out} for both devices. The results indicate that under this input power level, the optimized gain was 18.47 and 25.40 dB for conventional and TSC-HBT devices respectively. The higher gain of the cascode HBT, compared to the conventional device, appears to be due to the common–base stage providing additional power gain. The corresponding P_{out} was 18.11 and 22.98 dBm; PAE was 25.4%, 53.4% for each device. Compared with the PAE of conventional HBTs at the low input-power level, the cascode HBTs have much higher PAE due to the contribution of the CB-stage. It is important to note that TSC-HBT was able to maintain PAE values greater than 50% for a wide range of P_{in} values (−1 to 12 dBm). The peak efficiency of 60% was maintained across a wide power range also ($5 < P_{in} < 12$ dBm).

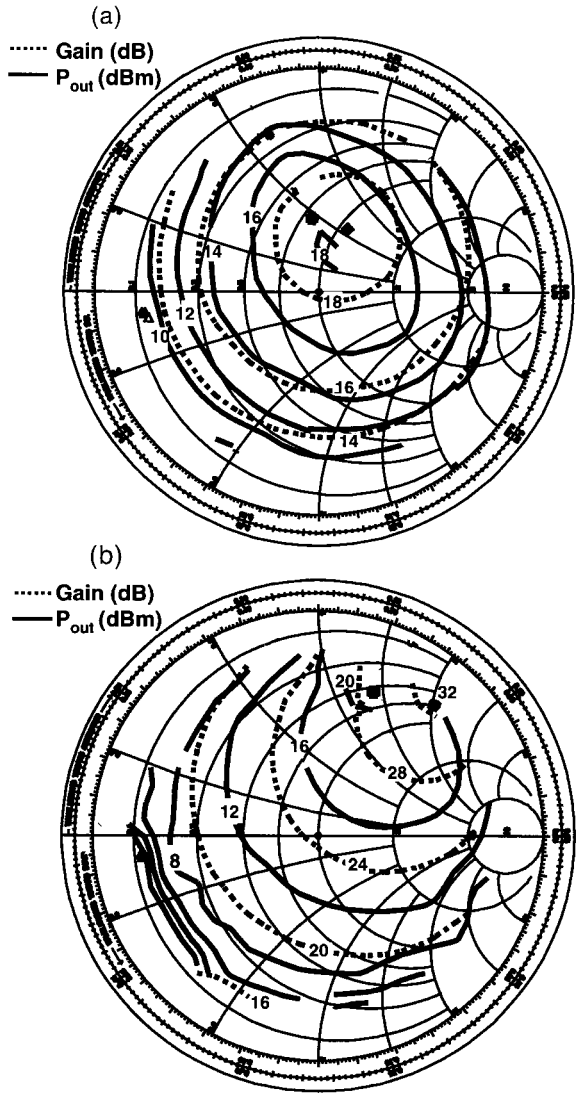

Fig. 6. 1-dB gain compressed on-wafer load pull measurement of (a) conventional HBTs: maximum gain = 18.5 dB and $P_{out}=18.2$ dBm; (b) cascode HBTs: maximum gain = 32.9 dB and $P_{out}=21.2$ dBm.

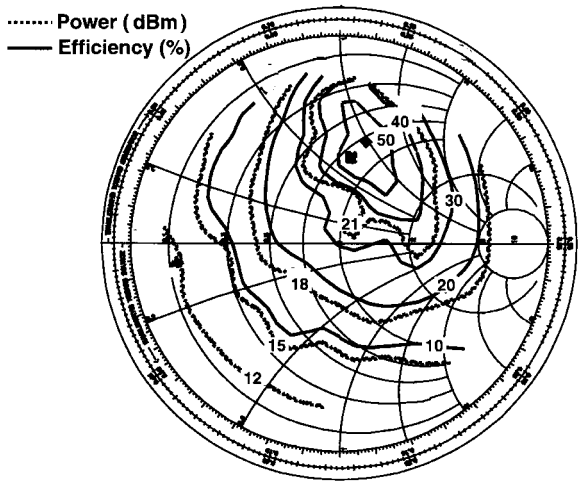

Fig. 7. P_{out} and PAE contours for cascode HBTs under large-signal conditions. Maximum $P_{out} = 23.4$ dBm at $\Gamma_L = 0.43\angle 81.7°$; maximum PAE = 60% at $\Gamma_L = 0.52\angle 74.9°$.

The power handling capability was investigated by measuring the 1 dB-gain compression characteristics of each device type. The measured power and gain characteristics are shown in Fig. 6 for the conventional and TSC-HBTs. As can be seen, the maximum compressed gain is 18.5 dB for conventional HBTs at $\Gamma_L = 0.34\angle 70.2°$, maximum $P_{out} = 18.2$ dBm at $\Gamma_L = 0.34\angle 94.4°$. On the other hand, the cascode device can reach a gain of 32.9 dB at $\Gamma_L = 0.79\angle -129.2°$ while producing $P_{out} = 21.2$ dBm at $\Gamma_L = 0.79\angle -129.2°$.

Fig. 7 shows the load-pull contour measurement results of the cascode device under high input-power level conditions. The load mismatch corresponded in this case to reflection coefficient of 0.9 and is therefore very close to the edge of the Smith Chart (VSWR = 19). The input power level was ~5 dBm and the device showed ~14 dB gain compression. It should be noted that the device could still operate with a maximum 60% of PAE under this highly gain-compressed condition. The purpose of stressing the devices with a high input power was to observe their stability under such conditions. As this figure shows, the contours for constant P_{out} and PAE are no longer uniform circles as under small-signal conditions. In addition, the optimum loads for maximum P_{out}, PAE and gain shifted toward the center of the Smith Chart compared to the positions observed under small-signal conditions. The distorted contour circles and Z_{opt} shift could be due to self-biasing, as well as, the presence of a very large collector voltage sweeping under large-signal conditions. In other words, the bias dependent elements such as C_{be} (I_c, V_{be}), C_{bc} (I_c, V_{bc}) appear to change with the input-power level. The cascode device was found to maintain its thermal stability even under these high gain compression and load-mismatched conditions. On the other hand, the conventional device

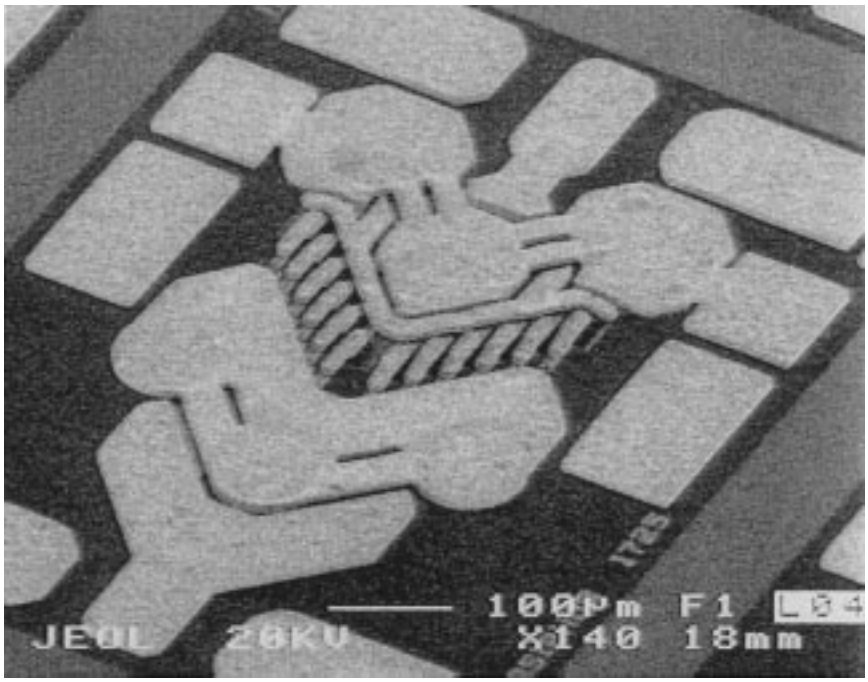

Fig. 8. SEM picture of a microwave high power TSC-HBT cell with 24 emitter fingers.

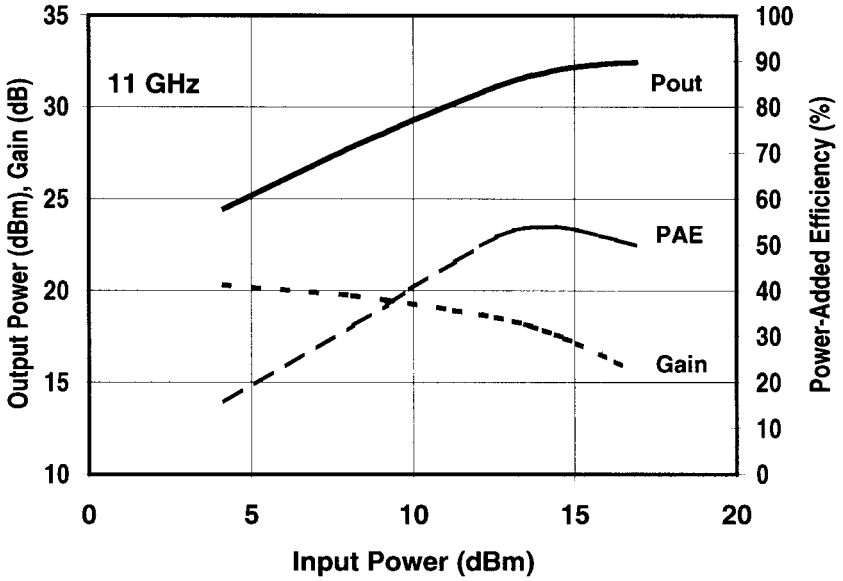

Fig. 9. Power performance of 24-finger TSC-HBT at 11 GHz with $V_{ce}=11$ V and $V_{b2}=2.5$ V.

was found to be thermally unstable under such strenuous gain compression conditions.

To identify the influence of the cascode CB-stage, load-pull measurements were performed on this stage alone. The results showed a relatively small variation of gain and P_{out} for different loads selected on the Smith Chart. This suggests that the power characteristics of the CB-stage are less sensitive to the matching condition provided by the output load. The load-pull measurement results led to the conclusion that the CB-stage of the cascode configuration improved thermal stability and relaxed the load-matching requirement of the device. Thus, we found that the TSC-HBT devices perform considerably better as microwave power amplifiers than conventional devices.

3.4. High power performance

We have employed relatively small size devices (4-fingers) to make a comparison between the conventional and TSC-HBT cells. The superior electrothermal properties demonstrated with small cells can only be useful in practice if such properties can be extended to higher power levels. At X-band frequencies, for example, typical HBT cells are expected to produce over 0.5 W and preferably over 1.0 W output power levels. To demonstrate that the TSC-HBT performance can be maintained as the devices are scaled up for higher power, we have fabricated a cell with 24 emitter fingers (in each of CE and CB stages) as shown in Fig. 8. A staggered layout approach was used in the design of this cell to minimize the thermal interaction between adjacent emitter fingers. The distance between CE and CB stages was kept constant at 100 μm, which means that identical staggering of fingers was used for both stages. Multiple bypass capacitors were used, as shown, to maintain uniform base grounding for the CB stage. The total width of the cell was only 300 μm.

The power performance of the high power cell is shown in Fig. 9. At 11 GHz, with $V_{ce}=11$ V and $V_{b2}=2.5$ V, the cell produced over 1.75 W CW output power with 17 dB gain and 55% PAE. This result, which is the highest reported for a HBT cell at this frequency with such high gain and efficiency, underscores the power capability of TSC-HBTs at microwave frequencies.

4. Conclusion

We have compared the DC, small-signal and large-signal power characteristics of conventional and TSC-HBTs and found that TSC-HBTs provide a higher power handling capability than conventional HBTs. The CB-stage in the TSC-HBTs not only leads to smaller temperature increase but also acts as an additional power amplification stage. The net result is that TSC-HBTs are eminently more suitable for high frequency power applications than conventional CE HBTs.

Acknowledgements

This work is supported by DARPA MAFET Thrust 2 Program, Contract No. N00014-95-C-6026.

References

[1] Gao G, Unlu MS, Morkoc H, Blackburn DL. IEEE Trans Electron Devices 1991;38:185.
[2] Liu W, Khatibzadeh A. IEEE Trans Electron Devices 1994;41:1698.
[3] Bayraktaroglu B, Barrette J, Kehias L, Huang CI, Fitch R, Neidhard R, Scherer R. IEEE Trans Electron Devices Lett 1993;14:493.
[4] Salib M, Bayraktaroglu B. IEEE MTT-S Int Microwave Symp Dig 1997;897.
[5] Zhang QM, Hu H, Sitch J, Surridge RK, Xu JM. IEEE Trans MTT 1996;44(11):2001.
[6] Lu K, Perry PA, Brazil TJ. IEEE Trans MTT 1995;43(7):1433.
[7] Samelis A, Pavlidis D. IEEE Trans MTT 1997;45(6): 886.